https://doi.org/10.3311/PPme.20234

Periodica Polytechnica Mechanical Engineering, 67(2), pp. 103–109, 2023

A Numerical Study of the Damage Mechanisms for CT Tensile Specimens of P265GH Steel Material

Mohammed Lahlou[1*], Abderrazak En-Naji[2], Nadia Mouhib[3], Bouchra Saadouki[4], Fatima Majid[5]

[1] Sciences for Energy Laboratory LabSIPE, ENSAJ, Chouaib Doukkali University, 24000 El Jadida, P.O.B. 1166, Morocco
[2] Laboratory M3ER, Department of Physics, Faculty of Sciences and Technology, Moulay Ismail University, 52003 Errachidia, P.O.B. 509, Morocco
[3] Laboratory of Mechanics, Higher Institute of Maritime Studies, Km 7 Road El Jadida, 20190 Casablanca, Morocco
[4] Laboratory of Control and Mechanical Characterization of Materials and Structures, National Higher School of Electricity and Mechanics, Hassan II University, 20190 Casablanca, P.O.B. 8118, Morocco
[5] Laboratory of Nuclear, Atomic, Molecular, Mechanical and Energetic Physics, University Chouaib Doukkali, 24000 El Jadida, P.O.B. 20, Morocco
* Corresponding author, e-mail: lahlou.m@ucd.ac.ma

Received: 27 March 2022, Accepted: 27 February 2023, Published online: 20 March 2023

Abstract

The aim of this paper is to determine the damage mechanisms of P265GH steel, commonly used for pressure equipment. First, an experimental study using tensile and Charpy tests allowed us to determine the mechanical properties (Young modulus E = 200 GPa, elongation ε = 35%, yield s_e = 320 MPa, ultimate stress s_u = 470 MPa, and K_{IC} = 96 MP√m). Then, numerical finite element modeling on a CT specimen using the CASTEM calculation code allowed us to determine the damage of the material when the notch depth varies. The analysis of the results shows that the numerical values of the stress concentration coefficient K_t and the stress intensity factor K_I are comparable with the analytically calculated values, thus validating our numerical study. The numerical results obtained revealed that the maximum stress σ_{max} is located in the vicinity of the notch bottom and the high probability density corresponds to a high loading level.

Keywords

pressure vessels, finite element model, stress concentration coefficient, notch, stress intensity factor

1 Introduction

Nowadays, the maintenance of pressure equipment in compliance with safety regulations is a major industrial issue. On the one hand, for reasons of improving industrial processes and taking into account energy and environmental concerns, the complexity of structures is increasing, either by their geometry, their stresses, or through the use of new materials [1]. On the other hand, in a context of profitability and rising raw material costs, over-conservatism is prohibited, and the thicknesses selected must be optimized. In this context, industrialists are always looking for new areas to explore in order to find efficient control tools that will allow them to determine the condition and lifetime of these structures [2].

All pressure equipment can present a significant risk in the event of failure [3, 4]. Researchers from the beginning of the 20th century tried to understand how a crack could lead to the failure of components. This task was not simple because cracks lead, in theory, to a mathematical singularity (the stresses and strains increase to infinity when approaching the crack front).

Griffith [5] was the first to highlight a term characterized by the loading and the associated criterion: when the crack is loaded, the stress field at the crack tip is proportional to the scalar. The Stress Intensity Factor is noted as K_I. If the loading increases and the material is brittle, K_I remains proportional to the loading, and the crack propagation appears when this factor reaches a critical value, characteristic of the material, noted K_{IC}.

El Hakimi et al. [6] investigated tubes having longitudinal or circumferential semi-elliptical flaws on the inner or outer surface. Jacquemoud et al. [7] used a nonlinear finite element computation in the elastoplastic domain to estimate the limiting pressure in a cylindrical shell with an inclined semi-elliptical defect and the J-integral. The J-integral can be calculated using the simplified estimate methods A16 and R6. Saffih and Hariri [8]

Cite this article as: Lahlou, M., En-Naji, A., Mouhib, N., Saadouki, B., Majid, F. "A Numerical Study of the Damage Mechanisms for CT Tensile Specimens of P265GH Steel Material", Periodica Polytechnica Mechanical Engineering, 67(2), pp. 103–109, 2023. https://doi.org/10.3311/PPme.20234

investigated the harmful effects of semi-elliptical circumferential or axisymmetric cracks in a cylindrical shell with a thickness transition (with the same inner diameter and different outer diameters). Allouti et al. [9] investigated the effect of sinking, specifically its depth, on the behavior of a tube under internal pressure. Meliani et al. [10, 11] attempts to determine and quantify the evolution of the Stress Intensity Factor and transverse stress. Yoshihara and Mizuno [12] investigated the critical stress intensity factor in simple notched specimens.

The aim of the article is to numerically analyze the evolution of stresses in the specimen's axis, the stress concentration coefficient, the stress intensity factor, the cracking speed, and the probability density for three loading levels (σ_a = 148 MPa, 284 MPa, 356 MPa for CT specimen).

2 Experimentation

2.1 Characterization test

Tensile tests were done at the Technical Center of Mechanical Industries Morocco (Cetim) to extract the mechanical characteristics of the P265GH steel that would be used in our program [13, 14]. Threaded specimens (Fig. 1) were obtained in the longitudinal and transverse orientations to examine the properties in the rolling direction. The stress versus elongation test curves is shown in Fig. 2.

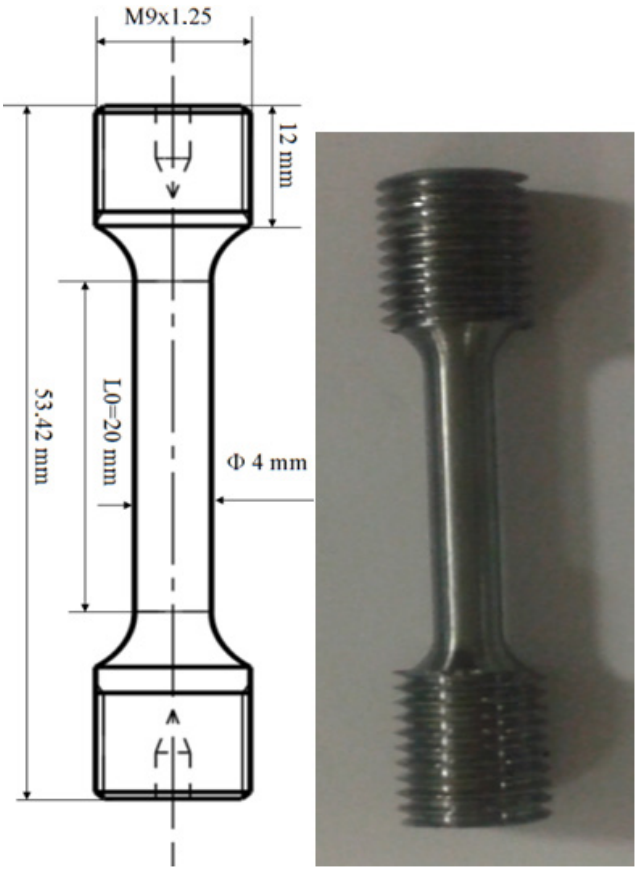

Fig. 1 Dimensions of the tensile test specimen

The main mechanical properties of P265GH steel, at ambient temperature, are shown in Table 1.

We note that the elongation is about 35%, which is higher than the 14% required by CODAP [15]. Therefore, this P265GH steel is well adapted for structures under pressure.

2.2 Charpy test

The Charpy test is a slow dynamic test that determines the effect of the strain rate on the mechanical properties of the materials, particularly toughness. The utilization of thermally activated plasticity in conjunction with the local failure condition causes this effect.

Fig. 3 [16] shows the geometry of the specimen used for the Charpy test.

The pendulum hammer's operation and the course of the tests follow a well-established procedure and adhere to current standards. Before each test campaign, three no-load tests are used to determine the hammer's friction. As shown in Fig. 4, a counter (angular dial of the machine) directly takes into account the value of the corresponding energy.

We performed two Charpy tests. The following precautions were taken:

- Place the specimen in the right position on its two support points.
- The specimen must not exhibit any fracture initiation.
- Check the normalization of the specimen.
- During the test, the temperature (in the laboratory) is stable and conforms.

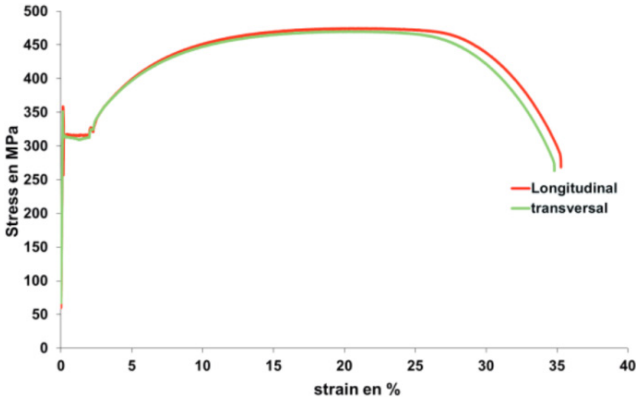

Fig. 2 Tensile curve

Table 1 Mechanical properties of the material

Young's modulus: E (GPa)	Yield stress: σ_e (MPa)	Ultimate stress: σ_g (MPa)	Elongation (%)	Poisson's ratio (ν)
200	320	470	35	0.3

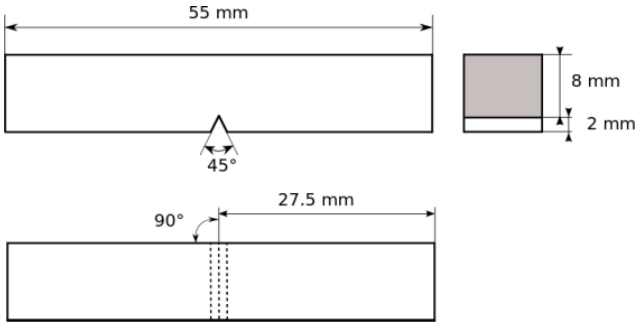

Fig. 3 Dimensions of Charpy impact test specimen

Fig. 4 Pendulum for Charpy test

The mean value of toughness associated with the resilience KCV is obtained by applying the Eq. (1) [17]:

$$\left(\frac{K_{IC}}{\sigma_e}\right)^2 = \frac{5}{\sigma_e}\left(\text{CVN} - \frac{\sigma_e}{20}\right), \quad (1)$$

where:

- K_{IC}: stress intensity factor in MPa√m;
- σ_e: Yield stress in MPa;
- CVN: Charpy energy in Joule.

We noted that CVN = 43.4 J, which gives the K_{IC} = 96 MPa√m.

3 Numerical modeling

The Cast3m computational code [18] is used to construct a finite element model for specimen analysis (CT). In the following, the finite element model is described.

3.1 Geometry

The specimen's geometry and dimensions are represented in Fig. 5 [19]. The specimen is stressed in tension in order to crack in open mode because the study is restricted to mode I.

3.2 Mesh and boundary conditions

Due to the symmetry of the problem, only half of the specimen is discretized. Because the numerical results are intended for fracture mechanics analysis, special attention is paid to the mesh, particularly at the crack's bottom and in its vicinity. Barsoum elements [20] are used with a very fine mesh to accomplish this. Fig. 6 illustrates the mesh in greater detail.

3.3 Loading

The simulated loading is a tensile stress along the longitudinal axis of the specimen. To reduce parasitic bending or twisting and to guarantee that the tensile tension is totally on axis, the tensile stress is given to the specimen through a rigid triangle, as illustrated by the arrow in Fig. 6. The selected loads are calibrated to apply nominal stresses of 148 MPa, 284 MPa, and 356 MPa, respectively.

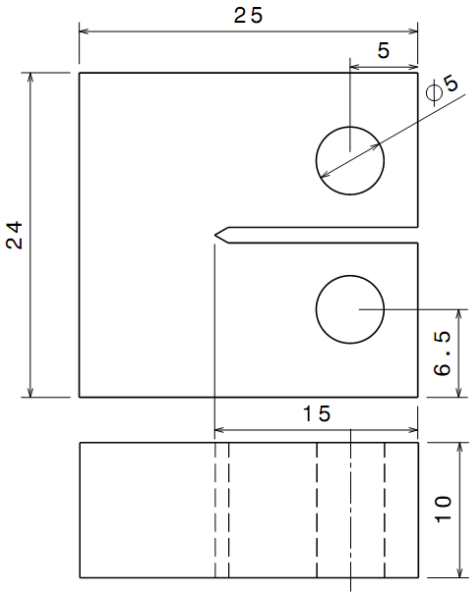

Fig. 5 Dimensions of the compact tension (CT) specimen (mm)

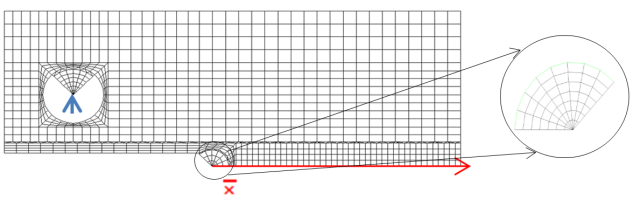

Fig. 6 Mesh of the CT specimen

4 Results and discussion

4.1 Stress evolution in the ligament

The curves in Fig. 7 show the evolution of the stress in the ligament of the specimen along the x-axis in Fig. 6 (the origin at the bottom of the crack) for the three applied stress levels: 148 MPa, 284 Mpa, and 356 Mpa.

The analysis of the curves in Fig. 7 shows that the maximum stresses are located at the bottom of the notch. We note that the stress gradually decreases with the distance from the bottom of the notch to stabilize at a stress equal to the nominal stress.

We distinguish three areas:

- The first area, which corresponds to stresses in the range [0, 320 Mpa]. The stress is lower than the elastic limit. This zone remains elastic.
- The second area, which corresponds to stresses in the range [320, 470 Mpa]. The stress is greater than the elastic limit of the material. The zone is the seat of plastic deformation.
- A third area, which corresponds to stresses (σ > 470 Mpa), generally near the bottom of the notch, where the stress exceeds the ultimate stress.

Table 2 represents a synthesis of the three remarkable values (maximum stress (s_{max}), minimum stress (s_{min}) and nominal stress (s_{nom}).

The numerical stress concentration factor Kt was defined by Peterson [21] using Eq. (2):

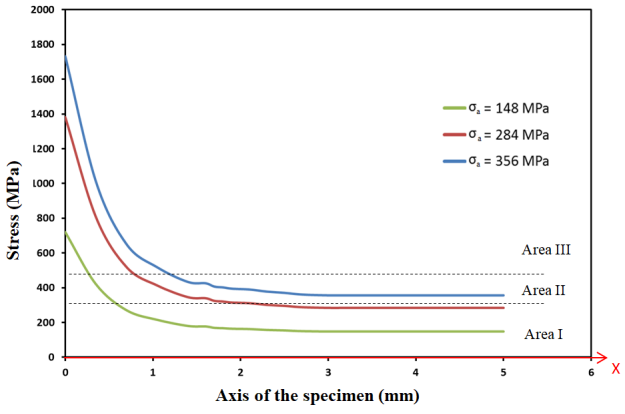

Fig. 7 Evolution of the Von Mises stress in the ligament of the specimen for the three levels of applied stress (σ_a = 356 Mpa, 284 Mpa, 148 Mpa)

Table 2 Numerical values of maximum stress (s_{max}), minimum stress (s_{min}), and nominal stress (s_{nom})

Applied stress (Mpa)	s_{max} (Mpa)	s_{min} (Mpa)	s_{nom} (Mpa)
148 Mpa	730	148	148
284 Mpa	1390	284	284
356 Mpa	1755	356	356

$$Kt_{num} = \frac{\sigma_{max}}{\sigma_{nom}}. \tag{2}$$

While François [22] used Eq. (3) to define the analytical stress concentration factor Kt:

$$Kt_{anal} = 1 + 2\sqrt{\frac{a}{r}}, \tag{3}$$

where:

- a: depth of notching;
- r: notch radius.

Table 3 shows the analytical (Kt_{anal}) and numerical (Kt_{num}) stress concentration factor values, as well as the relative error, which is the difference between the two values (Kt).

4.2 Evolution of the stress intensity factor

The calculation of the stress intensity factor depends on the geometry of the specimen [23, 24]. So for the CT specimen, we use Eq. (4) [25] in order to determine the evolution of the analytical K_I and compare it with the numerical K_I.

$$K_I = \frac{F}{t\sqrt{w}}\left[29.6\left(\frac{a}{w}\right)^{\frac{1}{2}} - 185.5\left(\frac{a}{w}\right)^{\frac{3}{2}} + 655.7\left(\frac{a}{w}\right)^{\frac{5}{2}} - 1017\left(\frac{a}{w}\right)^{\frac{7}{2}} + 638.9\left(\frac{a}{w}\right)^{\frac{9}{2}}\right], \tag{4}$$

where:

- K_I: stress intensity factor;
- F: applied force;
- t: the specimen's thickness;
- a: Depth of notching;
- w: the specimen's width.

The curves in Fig. 8 show the evolution of the numerical and analytical stress intensity factors (Eq. (4)) in the specimen ligament, i.e., along the x-axis in Fig. 6 (origin at the crack bottom) for the three applied stress levels: σ_a = 148 MPa, 284 MPa, and 356 MPa.

Analysis of the curves in Fig. 8 shows that there is a significant increase in the stress intensity factor as a function of crack length and applied stress.

Table 3 Analytical (Kt_{anal}) and numerical (Kt_{num}) stress concentration factor values

Applied stress (Mpa)	Kt_{num}	Kt_{anal}	Relative error
148	4.93	5	1.35%
284	4.89	5	2.11%
356	4.92	5	1.51%

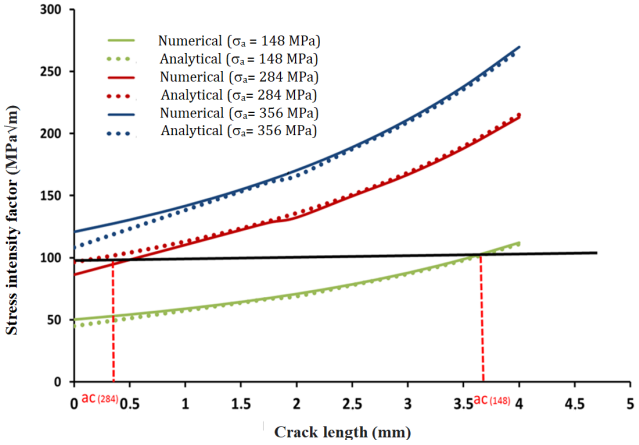

Fig. 8 Evolution of stress intensity factor K_I

The numerical stress intensity factor varies similarly to the analytical one.

Table 4 shows the critical crack length (a_c) and the relative error between the numerical and analytical Stress Intensity Factor values.

4.3 Evolution of the propagation speed

When a crack appears, its length grows with the number of cycles [26]. The cracking speed is calculated using Eq. (5):

$$\frac{da}{dN} = C\left(\Delta K\right)^m, \tag{5}$$

with:

- da/dN: cracking rate (where a is the crack length and N is the number of cycles applied);
- ΔK: stress intensity factor;
- C and m: material constants.

In our material, $C = 3.6 \times 10^{-10}$ and $m = 3$ [27].

The crack speed increases without preventing it until the specimen ruptures suddenly. Cracking is classified into three macroscopic stages:

- Stage I (propagation speed less than 10^{-3} mm/cycle);
- Stage II (propagation speed ranging from 10^{-5} to 10^{-3} mm/cycle);
- Stage III (rapid propagation leading to sudden rupture greater than 10^{-3} mm/cycle).

The curves in Fig. 9 show the evolution of the cracking speed according to the propagation of the crack.

Table 4 Values of critical crack lengths (a_c)

Applied stress (MPa)	a_c (mm)	Relative error
148 MPa	3.6	0.57%
284 MPa	0.4	0.76%
356 MPa	–	1.32%

Analysis of these results shows that there is a parabolic increase in cracking rate as a function of crack length and applied stress.

The stages of fracture propagation are shown in Table 5.

4.4 Failure probability density of the specimens studied

The WEIBULL distribution is applicable to buildings with minor problems. It was originally employed in the research of material fatigue, and it was extremely beneficial in the analysis of failure distributions of vacuum tubes. It is now virtually universally utilized in reliability.

The Weibull distribution is defined as (Eq. (6)):

$$f\left(x\right) = \frac{\beta}{\eta}\left(\frac{x-\gamma}{\eta}\right)^{\beta-1} e^{\left(\frac{x-\gamma}{\eta}\right)^{\beta}}, \tag{6}$$

with:

- γ: origin offset;
- β: shape parameter;
- η: scale parameter.

Its distribution function is denoted by the Eq. (7):

$$F\left(x\right) = 1 - e^{\left(\frac{x-\gamma}{\eta}\right)^{\beta}}, \tag{7}$$

As a result, the probability density [28] as a function of notch size is (Eq. (8)):

$$f\left(a\right)_{a_i} = \frac{1}{a_i} e^{-\left(\frac{a}{a_i}\right)^{\beta}}, \tag{8}$$

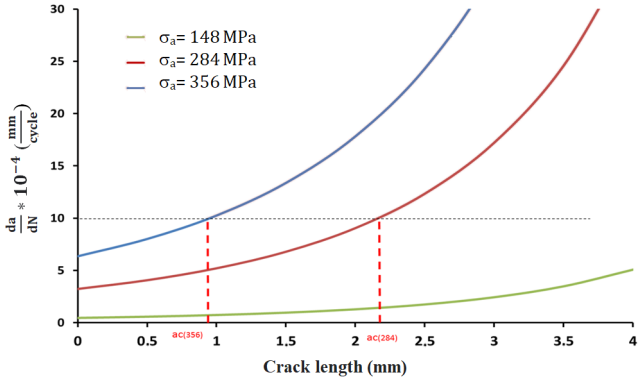

Fig. 9 The evolution of the crack speed

Table 5 Stages of crack propagation

Applied stress (MPa)	Stage I and II	Stage III
148 MPa	[0 5.2]	> 5.2
284 MPa	[0 2.2]	> 2.2
356 MPa	[0 0.9]	> 0.9

where:

- a_i: $a_{average}$ or $a_{critical}$ or $a_{priming}$;
- $a_{average}$: is the mean value of the crack size;
- $a_{critical}$: is the critical length of the crack;
- $a_{priming}$: is the length of the crack initiated (notch).

The results given in Fig. 10 show the probability densities calculated for the three parameters in crack length.

Fig. 10 shows that as the fracture length rises, the predicted probability density of failure reduces significantly. The intersection of the curves representing the probability density for the critical crack length ($a_{critical}$) and the crack length ($a_{priming}$) marks the end of Stage I, while the intersection of the curves representing the crack lengths ($a_{average}$) and ($a_{critical}$) marks the end of Stage II and the start of Stage III.

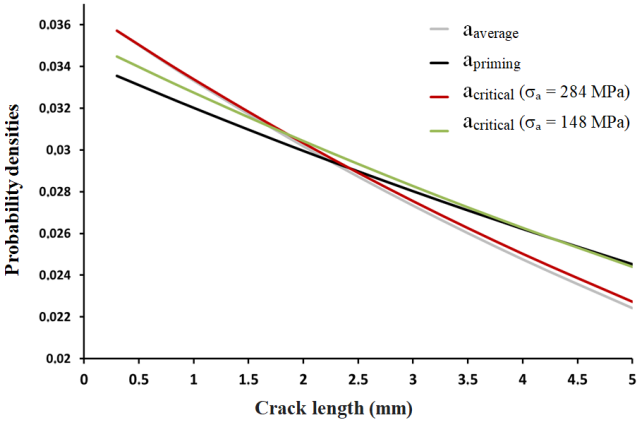

Fig. 10 Probability density function of the crack length

5 Conclusion

In the field of dangerous structures, such as pressure equipment, knowing the level of the defect's harmfulness is essential. The finite element approach to numerical modeling is a particularly efficient tool for solving this problem.

We developed a numerical model using Cast3m of a CT specimen to investigate the evolution of stress and stress intensity factors in the specimen's ligament for three levels of applied stress (σ_a = 356 MPa, 284 MPa, 148 MPa). We observe that all three stress curves exhibit a parabolic evolution to stabilize at a value equal to the applied stress for all results. The maximum stress is found towards the bottom of the notch. As the stress increases, the length of the critical notch diminishes. The cracking speed and probability densities allow us to anticipate the reliability of our material by determining the damage stages.

The finite element model that we used in our research is widely used and can be adapted for practical applications.

References

[1] Moustabchir, H., Elhakimi, A., Hariri, S., Azari, Z. "Pressure study of gas transport pipes, in the presence of defects notch type", presented at 18 ème Congrès Français de Mécanique, Grenoble, France, Aug. 27–31., 2007.

[2] Porziani, S., Augugliaro, G., Brini, F., Brutti, C., Chiappa, A., Groth, C., Mennuti, C., Quaresima, P., Salvini, P., Zanini, A., Biancolini, M. E. "Structural integrity assessment of pressure equipment by Acoustic Emission and data fractal analysis", Procedia Structural Integrity, 25, pp. 246–253, 2020. https://doi.org/10.1016/j.prostr.2020.04.029

[3] Qi, L.., Zhongbao, Q., Zijie, Z., Yiyi, L., Jianfeng, G., Qian, L. "Detection of parallel double crack in pressure vessel based on optical fibre ultrasonic sensing", Optical Fiber Technology, 68, 102784, 2022. https://doi.org/10.1016/j.yofte.2021.102784

[4] Ananda Rao, M., Sekhar Babu, R., Pavan Kumar, M. V. "Stress corrosion cracking failure of a SS 316L high pressure heater tube", Engineering Failure Analysis, 90, pp. 14–22, 2018. https://doi.org/10.1016/j.engfailanal.2018.03.013

[5] Griffith, A. A. "VI. The Phenomena of Rupture and Flow in Solids", Philosophical Transactions of the Royal Society A: Mathematical, Physical and Engineering Sciences, 221(582–593), pp. 163–198, 1921. https://doi.org/10.1098/rsta.1921.0006

[6] El Hakimi, A., Le Grognec, P., Hariri, S. "Numerical and analytical study of severity of cracks in cylindrical and spherical shells", Engineering Fracture Mechanics, 75(5), pp. 1027–1044, 2008. https://doi.org/10.1016/j.engfracmech.2007.04.027

[7] Jacquemoud, C., Delvallée-Nunio, I., Nédélec, M., Balestreri, F. "Additional Data Concerning French PWR RPV Steel to Evaluate the Relevance of a Size Effect Correction on Toughness in the Ductile-to-Brittle Transition", In: ASME 2014 Pressure Vessels and Piping Conference, Anaheim, CA, USA, 2014, V007T07A020. ISBN 978-0-7918-4606-3 https://doi.org/10.1115/PVP2014-28403

[8] Saffih, A., Hariri, S. "Numerical study of elliptical cracks in cylinders with a thickness transition", International Journal of Pressure Vessels and Piping, 83(1), pp. 35–41, 2006. https://doi.org/10.1016/j.ijpvp.2005.10.002

[9] Allouti, M., Schmitt, C., Pluvinage, G. "Assessment of a gouge and dent defect in a pipeline by a combined criterion", Engineering Failure Analysis, 36, pp. 1–13, 2014. https://doi.org/10.1016/j.engfailanal.2013.10.002

[10] Meliani, M. H., Azari, Z., Pluvinage, G., Matvienko, Y. G. "Variation of material failure curve with constraint", Procedia Engineering, 10, pp. 710–715, 2011. https://doi.org/10.1016/j.proeng.2011.04.118

[11] Meliani, M. H., Azari, Z., Pluvinage, G., Capelle, J. "Gouge assessment for pipes and associated transferability problem", Engineering Failure Analysis, 17(5), pp. 1117–1126, 2010. https://doi.org/10.1016/j.engfailanal.2010.01.007

[12] Yoshihara, H., Mizuno, H. "Mode I Critical Stress Intensity Factor of Medium - Density Fiberboard Obtained by Single-Edge - Notched Bending Test", Drvna Industrija, 65(2), pp. 99–104, 2014. https://doi.org/10.5552/drind.2014.1326

[13] Lahlou, M., Saadouki, A., En-naji, A., Majid, F., Mouhib, N. "A numerical study of the damage mechanisms of the specimens (SENT, SENB, CT, and DENT) used for P265 GH steel", Reliability: Theory & Applications, 17(3), pp. 72–81, 2022. https://doi.org/10.24412/1932-2321-2022-369-72-81

[14] Lahlou, M., Mouhib, N., Ouaomar, H., Hachim, A., Elghorba, M. "Numerical Study of Internal Radius Effect on Mechanical Behavior of P265GH Material", Periodica Polytechnica Mechanical Engineering, 60(4), pp. 233–237, 2016. https://doi.org/10.3311/PPme.8978

[15] Manufacturer members of the SNCT "CODAP Code de Construction des Appareils à Pression non soumis à la flame" (CODAP: Code for Construction of unfired Pressure Vessels), CODAP Steering Committee, France, 2005. (in French)

[16] Jian, F., Fulian, D., Chengzhong, W. "Experimental study on the material dynamic fracture properties by instrumented Charpy impact test with single specimen method", Journal de Physique Archives IV France, 110, pp. 551–557, 2003. https://doi.org/10.1051/jp4:20020751

[17] Barsom, J. M., Rolfe, S. T. "Stress analysis for members with cracks", In: Fracture and Fatigue Control in Structures: Application of Fracture Mechanics, ASTM, 1999, pp. 30–47. ISBN 978-0-8031-2082-2 https://doi.org/10.1520/MNL41-3RD-EB

[18] Cast3M "Cast3M: code d'éléments finis" (Cast3M: finite element code), [online] Available at: http://www-cast3m.cea.fr/ [Accessed: 01 January 2013] (in French)

[19] Martins, R. F., Ferreira, L. "Stress intensity factors KI, KII, KIII, Keq, induced at the crack tip of CT specimens subjected to torsional loading", Procedia Structural Integrity, 28, pp. 74–83, 2020. https://doi.org/10.1016/j.prostr.2020.10.010

[20] Barsoum, R. S. "Further application of quadratic isoparametric finite elements to linear fracture mechanics of plate bending and general shells", International Journal of Fracture, 11(1), pp. 167–169, 1975. https://doi.org/10.1007/BF00034724

[21] Peterson, R. E. "Stress concentration factors: Charts and relations useful in making strength calculations for machine parts and structural elements", Wiley, 1974. ISBN 0471683299

[22] François, D. "Endommagement et la rupture des materiaux" (Damage and failure of materials), EDP Sciences, 2004. ISBN 2-86883-714-X (in French)

[23] Zekriti, N., Rhanim, R., Majid, F., Lahlou, M., Ibrahim, M., Rhanim, H. "Mode I stress intensity factors of printed and extruded specimens based on Digital Image Correlation method (DIC): case of ABS material", Procedia Structural Integrity, 28, pp. 1745–1754, 2020. https://doi.org/10.1016/j.prostr.2020.10.149

[24] Majid, F., Zekeriti, N., Rhanim, R., Lahlou, M., Rhanim, H., Mrani, B. "Mechanical behavior and crack propagation of ABS 3D printed specimens", Procedia Structural Integrity, 28, pp. 1719–1726, 2020. https://doi.org/10.1016/j.prostr.2020.10.147

[25] Duggan, T. V., Proctor, M. W., Spence, L. J. "Stress intensity calibrations and compliance functions for fracture toughness and crack propagation test specimens", International Journal of Fatigue, 1(1), pp. 37–47, 1979. https://doi.org/10.1016/0142-1123(79)90043-4

[26] Pomey, G. "Les différents domaines de la fatigue des métaux et les paramètres de l'endurance des Pièces" (The different areas of metal fatigue and the endurance parameters of parts), In: 15 colloque de métallurgie spéciale, City of conference, Country, 1972, pp. 26–75. (in French)

[27] El Ghobra, M. "Évolutions du dommage et de la propagation de la fissure sous chargement cyclique de l'acier A36 et l'aluminium 6351-T6" (Evolutions of damage and crack propagation under cyclic loading of A36 steel and 6351-T6 aluminum), MSc Thesis, École Polytechnique de Montréal, 1985. (in French)

[28] Hachim, A., Farid, H., El Ghorba, M., El Had, K., Akef, A., Chergui, M. "The probability density of stress intensity factor in S355 Steel", Research Inventy: International Journal of Engineering and Science, 1(2), pp. 12–15, 2012. [online] Available at: https://www.researchinventy.com/papers/v1i2/C012012015.pdf [Accessed: 26 March 2022]